Evaluating Learning Potential with Internal States in Deep Neural Networks

Shogo Takasaki and Shuichi Enokida
Graduate School of Computer Science and Systems Engineering, Kyushu Institute of Technology, 680-4 Kawazu, Iizuka-shi, Fukuoka, 820-8502, Japan

Keywords: Deep Learning, Anticipating Accidents, Long Short-Term Memory, Evaluating Learning Potential.

Abstract: Deploying deep learning models on small-scale computing devices necessitates considering computational resources. However, reducing the model size to accommodate these resources often results in a trade-off with accuracy. The iterative process of training and validating to optimize model size and accuracy can be inefficient. A potential solution to this dilemma is the extrapolation of learning curves, which evaluates a model's potential based on initial learning curves. As a result, it is possible to efficiently search for a network that achieves a balance between accuracy and model size. Nonetheless, we posit that a more effective approach to analyzing the latent potential of training models is to focus on the internal state, rather than merely relying on the validation scores. In this vein, we propose a module dedicated to scrutinizing the network's internal state, with the goal of automating the optimization of both accuracy and network size. Specifically, this paper delves into analyzing the latent potential of the network by leveraging the internal state of the Long Short-Term Memory (LSTM) in a traffic accident prediction network.

1 INTRODUCTION

Deep Neural Networks (DNNs) have achieved remarkable results across various fields such as image recognition and natural language processing in recent years. Deploying deep learning models on automobiles and robots paves the way for autonomous driving and human-supporting robots. However, the constraint of equipping such robots with large-scale computing servers makes the use of edge computing devices more desirable. Nonetheless, edge computing devices pose significant resource limitations, such as CPU and GPU capabilities, necessitating consideration of the size of the deployed deep learning models. Reducing the model size appears to be a solution, yet it incurs a trade-off between accuracy and network size, making it imperative to design networks that harmonize accuracy with network size.

The most straightforward approach to optimal network exploration involves trial and error through repeated training and validation, but the expansive search space due to various hyperparameter combinations renders this approach inefficient. Besides, the repetitive training and accuracy validation up to the set epochs incur significant time and computational resource costs. Hence, predicting the network's future performance early in training becomes crucial. Learning Curve Extrapolation (LCE) (Swersky et al., 2014; Domhan et al., 2015; Klein et al., 2017)emerges as a method to evaluate a network's potential early in training. While human experts typically evaluate a model's potential by inspecting the learning curves, LCE extrapolates the end of the learning curves from the early ones to assess a model's potential. LCE enables the evaluation of a model's potential at an early stage, facilitating efficient training for models where high diversity is anticipated. Lately, LCE has found application in the realm of Neural Architecture Search (NAS).

NAS, an AutoML (Hutter et al., 2019) technique, automates the identification of optimal neural network architectures and has made significant impacts across diverse domains like image classification (Zoph et al., 2018; Real et al., 2019), object detection (Chen et al., 2019; Wang et al., 2020) and semantic segmentation (Zhang et al., 2019; Liu et al., 2019). Core elements of NAS encompass the search space, search strategy, and performance estimation. In this framework, a search strategy selects a structure A from Search Space $\mathcal{A}$ and assesses its performance, iterating this selection and evaluation to optimize the neural network architecture. Given the

Takasaki, S. and Enokida, S.
Evaluating Learning Potential with Internal States in Deep Neural Networks.
DOI: 10.5220/0012298500003660
Paper published under CC license (CC BY-NC-ND 4.0)
In *Proceedings of the 19th International Joint Conference on Computer Vision, Imaging and Computer Graphics Theory and Applications (VISIGRAPP 2024) - Volume 2: VISAPP*, pages 317-324
ISBN: 978-989-758-679-8; ISSN: 2184-4321
Proceedings Copyright © 2024 by SCITEPRESS – Science and Technology Publications, Lda.

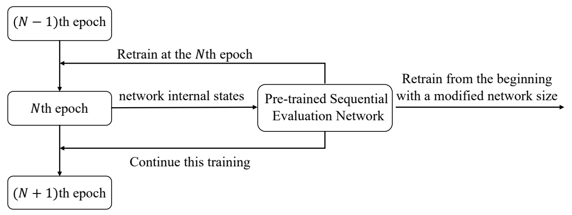
$(N-1)$th epoch
Retrain at the Nth epoch
Retrain from the beginning with a modified network size
Nth epoch
network internal states
Pre-trained Sequential Evaluation Network
Continue this training
$(N+1)$th epoch

Figure 1: System overview utilizing the Sequential Evaluation Network (SEN). Upon completion of training at the N-th epoch, the internal parameters are fed into the pre-trained SEN, which subsequently outputs one of three states to autonomously control the training process: (i) Continue Training: The training continues if high future accuracy is anticipated with the current network size. (ii) Retrain the Current Epoch: If the training results from the current epoch adversely impact the internal state, retraining is initiated at the same epoch. (iii) Retrain with Adjusted Network Size: If the current network size is deemed to lack potential, the network size is expanded, and retraining begins anew.

plethora of networks NAS evaluates, efficient performance estimation becomes vital. LCE has emerged as an efficient strategy for performance estimation (Baker et al., 2018; Wistuba and Pedapati, 2019; Yan et al., 2021). Another notable direction in NAS optimizes for constraints typical of small computers, not merely accuracy. For example, FBNet (Wu et al., 2019) optimizes both accuracy and inference speed on mobile devices by introducing Differentiable Neural Network Architecture Search (DNAS) which employs an Operator Latency LUT to balance accuracy with inference speed.

As elaborated, assessing the model's potential early on proves beneficial for NAS tasks, emphasizing not only accuracy but also lightweightness. In this study, we aim to construct a Sequential Evaluation Network (SEN) that incrementally assesses a model's potential. SEN strives for balanced learning in terms of accuracy and network size by evaluating the model's potential during training and autonomously controlling the training process. Our approach distinctively centers on the network's internal state rather than on validation accuracy, akin to LCE. We posit that by honing in on the internal state, we can gauge the latent potential of a model, unreflected in the network output, enabling more efficient training control. Moreover, computing validation accuracy every epoch using large datasets and metrics such as Average Precision (AP) can be resource-intensive. In contrast, SEN, bypassing validation accuracy, assesses the model's potential in a more lightweight manner. Figure 1 illustrates the system overview using SEN. Training initiates with an extremely small network size, expanding until SEN anticipates higher accuracy in the future, thereby efficiently training a model that balances accuracy and network size.

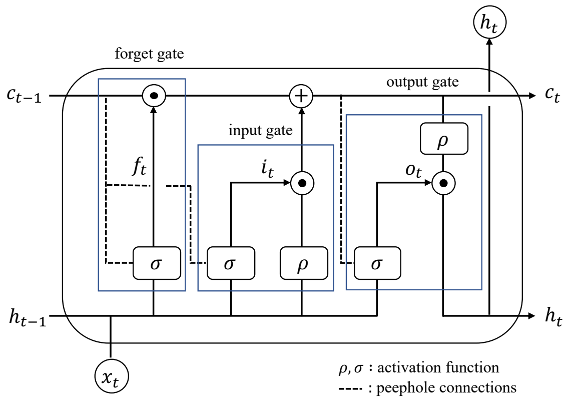

Figure 2: Schematic of an LSTM block, illustrating data flow through input, forget, and output gates along with the memory cell. Equations (1)–(6) describe the interactions and updates within the block.

In this paper, as a foundamental study for constructing SEN, we explore a traffic accident prediction network employing onboard monocular camera footage as our subject of investigation. One such network is the Dynamic Spatial Attention - Recurrent Neural Network (DSA-RNN) (Chan et al., 2016). DSA-RNN chiefly consists of an image feature extraction component and a temporal data processing component. Generally, CNNs used for image feature extraction in such systems leverage pretrained models, with training commonly reserved for the temporal data processing network. Consequently, In this study, our aim is to optimize the accuracy and network size of LSTM (Long Short-Term Memory) used for processing time-series data. To achieve this, we closely examine the internal states of the LSTM and aim to evaluate the potential of the model during training on a step-by-step basis.

2 RELATED WORK

2.1 LSTM

Recurrent Neural Networks (RNNs) are commonly cited as foundamental architectures for processing time series data. These networks possess a unique structure characterized by self-recursive connections across time. Specifically, the intermediate activation feature $\boldsymbol{h}_{t-1}$ from a given timestep is integrated with the input $\boldsymbol{x}_t$ of the subsequent timestep. Although RNNs are engineered to process time series data, they suffer from the vanishing gradient problem (Pascanu et al., 2013), which hampers long-term learning. LSTM addresses this issue by substituting the hidden layer nodes with LSTM blocks, as illustrated in Figure 2.

LSTM is architected around a Constant Error Carousel (CEC, also known as a memory cell), an input gate, a forget gate, and an output gate. The memory cell in an LSTM retains information over multiple time steps. The forget gate determines the fraction of long-term memory from the preceding time step to retain, while the input gate decides the amount of current input or short-term memory to store in the memory cell, effectively updating its state. The output gate then decides how much information should be emitted based on the current internal state. The output at time t is recurrently used as input for the LSTM block at the subsequent timestep $t+1$. As illustrated in Figure 2, the input at time t is represented by $\boldsymbol{x}_t$, and the output is denoted by $\boldsymbol{h}_t$.

Assuming the quantity of LSTM blocks is N and the number of inputs is M, the weight, serving as the learning parameter, is described as:

- Input weights: $\boldsymbol{W}_z, \boldsymbol{W}_f, \boldsymbol{W}_i, \boldsymbol{W}_o \in \mathbb{R}^{N\times M}$
- Recurrent weights: $\boldsymbol{R}_z, \boldsymbol{R}_f, \boldsymbol{R}_i, \boldsymbol{R}_o \in \mathbb{R}^{N\times N}$
- Peephole connection weights: $\boldsymbol{p}_f, \boldsymbol{p}_i, \boldsymbol{p}_o \in \mathbb{R}^{N}$
- Bias: $\boldsymbol{b}_z, \boldsymbol{b}_f, \boldsymbol{b}_i, \boldsymbol{b}_o \in \mathbb{R}^{N}$

Moreover, the variables $\boldsymbol{z}_t$, $\boldsymbol{f}_t$, $\boldsymbol{i}_t$, $\boldsymbol{o}_t$, and $\boldsymbol{c}_t$ correspond to the input to the LSTM block, the forget gate, the input gate, the output gate, and the memory cell at time t, respectively. These are defined by the following equations:

$$\boldsymbol{z}_t = \rho(\boldsymbol{W}_z\boldsymbol{x}_t + \boldsymbol{R}_z\boldsymbol{h}_{t-1} + \boldsymbol{b}_z) \quad (1)$$
$$\boldsymbol{f}_t = \sigma(\boldsymbol{W}_f\boldsymbol{x}_t + \boldsymbol{R}_f\boldsymbol{h}_{t-1} + \boldsymbol{p}_f \odot \boldsymbol{c}_{t-1} + \boldsymbol{b}_f) \quad (2)$$
$$\boldsymbol{i}_t = \sigma(\boldsymbol{W}_i\boldsymbol{x}_t + \boldsymbol{R}_i\boldsymbol{h}_{t-1} + \boldsymbol{p}_i \odot \boldsymbol{c}_{t-1} + \boldsymbol{b}_i) \quad (3)$$
$$\boldsymbol{o}_t = \sigma(\boldsymbol{W}_o\boldsymbol{x}_t + \boldsymbol{R}_o\boldsymbol{h}_{t-1} + \boldsymbol{p}_o \odot \boldsymbol{c}_{t} + \boldsymbol{b}_o) \quad (4)$$
$$\boldsymbol{c}_t = \boldsymbol{z}_t \odot \boldsymbol{i}_t + \boldsymbol{c}_{t-1} \odot \boldsymbol{f}_t \quad (5)$$
$$\boldsymbol{h}_t = \rho(\boldsymbol{c}_t) \odot \boldsymbol{o}_t \quad (6)$$

In these equations, $\odot$ symbolizes the Hadamard product. Typically, the sigmoid function ($\sigma(x) = 1/(1+e^{-x})$) serves as the activation function for the gates, while the hyperbolic tangent function is utilized for both input and output activations.

Due to the incorporation of memory cells and diverse gates, LSTM can process extensive time series data more effectively than conventional RNNs. Hence, in recent times, deep learning techniques for time series data processing have found applications in various sectors, such as video and motion picture analysis, linguistic processing, and audio processing.

In the analysis of LSTM's internal parameters (Greff et al., 2017), the impact on performance when certain parameters are omitted is discussed. Notably, the performance degradation is substantial when removing the forget gate and the activation function of the output. This indicates that within the LSTM, the forget gate and the output's activation function play crucial roles. A visualization study of the LSTM (Karpathy et al., 2016) examined each LSTM cell's operation. It has been mentioned that LSTM cells, existing in multiple within the hidden layers, have variations in their behaviors. In particular, when focusing on the values of the forget gate, it has been reported that there are cells that operate to retain memory over a long period of time. However, some cells are not easily interpretable. Therefore, we assume that models with a higher proportion of highly active cells amidst a mixture of highly and less active cells in the hidden layer have potential for the future. We define the activity level of LSTM cells using the value of the forget gate, which has been reported to particularly contribute to accuracy.

2.2 Traffic Accident Prediction Using DSA-RNN

Figure 3 presents the model visualization of DSA-RNN, which is designed to predict traffic accidents using an LSTM based on information acquired from an onboard monocular camera. The input to the DSA-RNN at time t is a frame image whose features $\boldsymbol{x}_t^F$ are generated by passing the frame through a CNN. Although these frame features capture the overall characteristics of the image, they might not effectively capture the details of objects, such as four-wheeled or two-wheeled vehicles, appearing only in parts of the image.

In order to address this limitation, the Dynamic Spatial Attention (DSA) mechanism is proposed to extract object features $\boldsymbol{x}_t^D$ focused on potentially hazardous objects within the image. By providing the LSTM with both the object features $\boldsymbol{x}_t^D$ extracted by the DSA and the frame features $\boldsymbol{x}_t^F$, the surrounding environment is considered during traffic accident prediction.

The features of each potentially hazardous object detected by Faster R-CNN (Ren et al., 2015) are represented as $\hat{\boldsymbol{x}}_t^j$, and the importance of each hazardous object is given by α_t^j. Here, J denotes the number of potentially hazardous objects, with j indexing each object from 1 to J. The object features $\boldsymbol{x}_t^D$ obtained by the DSA are computed as in Equation (7), where the importance of each object α_t^j is computed according

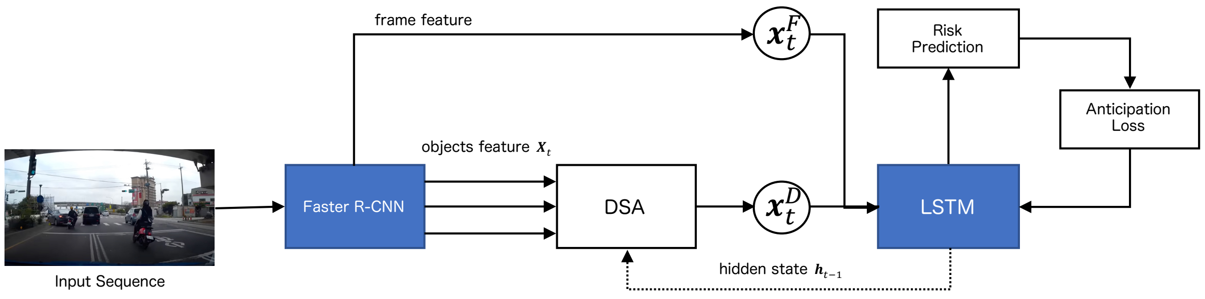

Figure 3: Architecture of the DSA-RNN model, integrating frame features, $\boldsymbol{x}_t^F$, and dynamically-attended object features, $\boldsymbol{x}_t^D$, for traffic accident prediction using the LSTM and onboard monocular camera inputs.

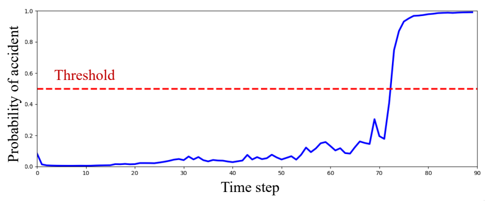

Figure 4: Temporal evolution of the DSA-RNN's predicted accident probability (solid blue line) across sequential frames, triggering an accident prediction when exceeding a predefined threshold (red dashed line).

to Equation (8). In Equation (8), the term e_t^j is calculated as shown in Equation (9). In this formulation, $\boldsymbol{w}$, $\boldsymbol{W}_e$, $\boldsymbol{U}_e$, and $\boldsymbol{b}_e$ are training parameters, and $\boldsymbol{h}_{t-1}$ represents the activation feature of the LSTM from the preceding time step.

As shown in Figure 4, the network computes the probability of an accident at each time step. When the accident probability, represented by the solid blue line, surpasses the threshold indicated by the red dashed line, a traffic accident is predicted to occur in that scene.

$$\boldsymbol{x}_t^D = \mathrm{DSA}(\boldsymbol{X}_t, \boldsymbol{\alpha}_t) = \sum_{j=1}^{J} \alpha_t^j \hat{\boldsymbol{x}}_t^j \tag{7}$$

$$\alpha_t^j = \frac{\exp(e_t^j)}{\sum_j \exp(e_t^j)} \tag{8}$$

$$e_t^j = \boldsymbol{w}^T \rho(\boldsymbol{W}_e \boldsymbol{h}_{t-1} + \boldsymbol{U}_e \hat{\boldsymbol{x}}_t^j + \boldsymbol{b}_e) \tag{9}$$

3 PROPOSED METHOD

We assume that within the hidden layers where multiple LSTM cells exist, there is a mix of cells with high and low activity levels, and the higher the proportion of highly active cells, the more promising the model is. Therefore, we focus on the values of the LSTM's forget gate to define the activity level of the LSTM cells. Moreover, based on the aforementioned assumption, we define an overall activity level metric for the LSTM. This metric aggregates the activity level information across all LSTM cells and serves as an indicator of the model's potential. A mathematical formulation of the activity level metric, based on the forget gate values, could provide a quantifiable measure of the model's potential, enabling more objective evaluations and comparisons.

3.1 Definition of Highly Active LSTM Cells

The LSTM uses a forget gate to regulate the degree of memory retention from the previous time step. At time t, the forget gate $\boldsymbol{f}_t$ is an N-dimensional vector, where N denotes the number of nodes in the hidden layer, represented as $\boldsymbol{f}_t = (f_t^1 f_t^2 \dots f_t^N)^\top$. As indicated in Equation (5), if the value of the forget gate $f_t^k (k \in 1, \dots, N)$ is 1, the memory is entirely retained. Conversely, a value of 0 leads to complete memory forgetting. With appropriate timing of its forgetting mechanism, the LSTM can process considerably longer sequences compared to RNN and effectively handle changes in conditions. In accident prediction scenarios, a rapid decrease in the forget gate value might signify a transition from a safe to a hazardous situation. This allows the LSTM to integrate information in dangerous scenarios more effectively. Considering the operation of the forget gate, we discuss three types, as represented in Figures 5a to 5c. In these figures, the red solid line depicts the average transition of the forget gate value $\boldsymbol{f}_t$ for all cells, and the green solid line illustrates the transition of the forget gate value f_t^k for a specific cell. Figure 5a showcases a cell that maintains memory by persistently transitioning at values near its maximum. Figure 5b represents a cell mirroring the average transition of the forget gate value. Figure 5c typifies a cell with significant fluctuations, differing from the mean

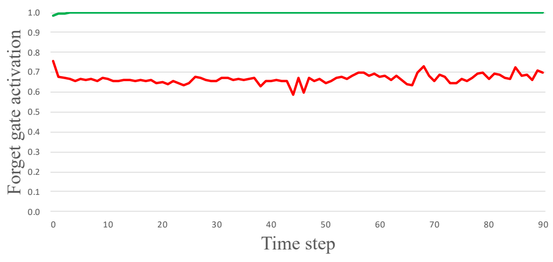

(a) Persistent Memory Retention

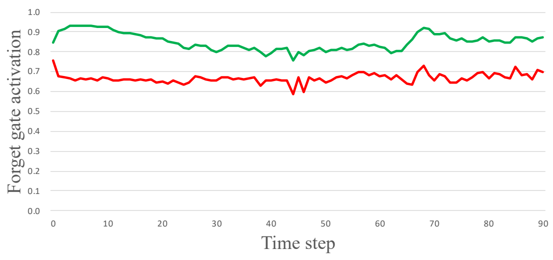

(b) Average Transition

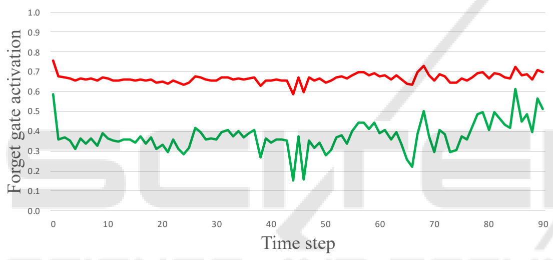

(c) Notable Fluctuations

Figure 5: Transitions of forget gate values of LSTM cells demonstrating different behaviors: (a) Persistent memory retention, (b) Typical average transition, and (c) Notable fluctuations representing responsiveness to situational changes. Red and green lines depict average and specific cell forget gate values, respectively.

transition. LSTM cells with pronounced fluctuations, such as those shown in Figure 5c, indicate their responsiveness to sudden situational changes.

Here, based on the magnitude of local variations in the values of the forget gate, we define the LSTM Cell Activity Level (LCAL). The LCAL of the LSTM cell k is defined in Equation (10). In the equation, $\mathrm{CV}_k(t)$ is the coefficient of variation of the values of the forget gate, as shown in Equation (11). The coefficient of variation is calculated for each moving average of window size w, as shown in Equation (12). When evaluating the variability of the forget gate's values solely by the standard deviation, it is believed that there would be little difference in the variability across windows. Therefore, by using the mean value, which is less than 1, to subtract from the standard deviation, a form of weighting is applied, making the differences in variability more pronounced. Furthermore, by calculating the variation using moving averages, we derive the local variation amount of the values of the forget gate, and define its maximum value as LCAL.

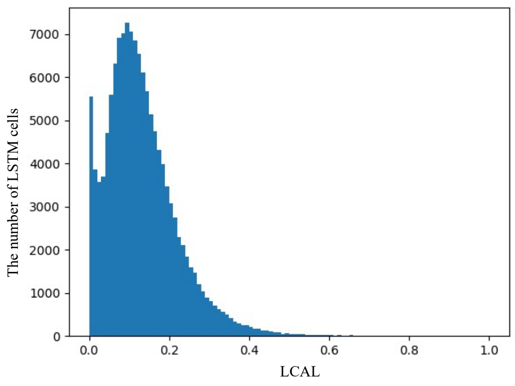

Figure 6: Histogram of LCAL across all LSTM cells for TrueP scenes. LCAL values are calculated for each of the $N \cdot \mathrm{TP}$ patterns arising from N hidden layers and TP TrueP scenes, revealing the distribution of activity levels within the network during accurate accident prediction. The LSTM Activity Level (LAL) is subsequently derived from these distributions, offering insight into the potential of the model based on the prevalence of high-activity LSTM cells.

$$\mathrm{LCAL}_k = \max_t \mathrm{CV}_k(t) \tag{10}$$

$$\mathrm{CV}_k(t) = \frac{\sqrt{\frac{1}{w}\sum_{i=t}^{t+w-1}(f_i^k - \mathrm{MA}_k(t)))^2}}{\mathrm{MA}(t)} \tag{11}$$

$$\mathrm{MA}_k(t) = \frac{1}{w}\sum_{i=t}^{t+w-1} f_i^k \tag{12}$$

3.2 Definition of the Overall Activity Level of LSTM

We assume that the higher the proportion of LSTM cells with a large LCAL when viewed across the entire hidden layer, the more potential the model has. Based on this assumption, we define the LSTM Activity Level (LAL). In the context of traffic accident prediction, we consider the scenes where the forget gate value is most activated to be the scenes where accidents are correctly predicted when they occur, and we denote such scenes as TrueP. We calculate the LCAL for all scenes that are TrueP. At this time, if we denote the total number of TrueP scenes as TP, then there exist TP states of hidden layers. In other words, if we denote the number of hidden layers as N, $N \cdot \mathrm{TP}$ patterns of LCAL are calculated. These LCALs are represented in a single histogram, as shown in Figure 6.

As shown in Figure 5a, the LCAL value of the cell is close to 0. Given this, we expect the LCAL histogram to be concentrated around the value of 0. Therefore, as shown in Equation (13), we define LAL as the proportion of LSTM cells with an LCAL greater than a threshold τ_{LAL}. Here, the function $\mathrm{I}(\cdot)$ acts as an indicator function, returning 1 if the condition is met and 0 otherwise.

$$\mathrm{LAL} = \frac{1}{N \cdot \mathrm{TP}} \sum_{k=1}^{N} \sum_{\mathrm{TrueP}=1}^{\mathrm{TP}} \mathrm{I}(\mathrm{LCAL}_k^{\mathrm{TrueP}} \geq \tau_{\mathrm{LAL}}) \tag{13}$$

4 EXPERIMENT

4.1 Experiment Details

In this section, we provide a detailed description of the preliminary experiments aimed at constructing SEN for traffic accident prediction. For this experiment, we utilized the Dashcam Accident Dataset (DAD) (Chan et al., 2016) and trained it for 30 epochs. Herein, we denote the models with hidden layer sizes set to 128, 512, 1024, and 2048 as M_{128}, M_{512}, M_{1024}, and M_{2048}, respectively. As LSTM's internal states change with each training iteration, we trained the M_{128}, M_{512}, M_{1024}, and M_{2048} models ten times each. Subsequently, we conducted preliminary experiments on these trained models using the analytical methods described in Section 3. The experiments were conducted using TensorFlow on a server equipped with an NVIDIA RTX A6000 GPU.

4.1.1 Details of the Dashcam Accident Dataset

The DAD consists of dashcam footage capturing vehicular and motorcycle accidents shot in Taiwan. Each video clip is recorded at 20fps, spanning 100 frames, or a total duration of 5 seconds. For clips containing accidents, the actual accident event is captured between the 90th and 100th frames. As a result, the 90 frames leading up to the accident are used to predict its occurrence. For this experiment, the dataset comprises a total of 620 videos with accidents (455 for training and 165 for validation) and 1,130 videos without accidents (829 for training and 301 for validation).

4.1.2 Evaluation Metrics

For evaluating the activity level of LSTM cells, we use the LCAL set with a window size $w = 5$. In the DAD dataset, as the last 10 frames of the accident-inclusive videos contain the actual accident, the interval (90, 100] is excluded from evaluation. Additionally, due to the network output's instability in the initial frames, the interval [1, 10) is also excluded. Therefore, the LCAL is calculated using the moving average in the interval [10,90]. Moreover, as an indicator of the model's potential, we use LAL with a threshold $\tau_{\mathrm{LAL}} = 0.05$.

For assessing the accuracy of traffic accident prediction, we use Average Precision (AP). In scenes containing an accident, the number of scenes correctly predicted to have an accident is termed True Positive (TP), while the number of scenes mistakenly predicted as non-accidental is labeled False Negative (FN). Conversely, in non-accident scenes, scenes incorrectly predicted to have an accident are designated as False Positive (FP), and those accurately predicted without an accident are labeled True Negative (TN). Using these metrics, Recall and Precision are computed for each accident threshold to derive the AP.

4.2 Results

4.2.1 Transition of LSTM Activity Levels

For the models M_{128}, M_{512}, M_{1024}, and M_{2048} trained 10 times each, we calculated LAL and AP at epochs 5, 10, 15, 20, 25, and 30. We then recorded the transition of the average LAL and AP over the epochs for each model. Notably, for some epochs of M_{128} and M_{512} (primarily at epoch 5), there were no scenes with TrueP, making it impossible to compute LAL. Hence, we plotted the average of the available LAL data. The transitions of LAL and AP are depicted in Figures 7 and 8, respectively.

When focusing on the AP of M_{128}, it is evident that the training was not very effective, registering the lowest value at epoch 30. On the other hand, by examining the LAL, its value was comparable to other models during the early training phases. However, as training progressed, there was minimal growth, setting at a lowest value by epoch 30. The fluctuations in AP suggest that the number of LSTM cells may be insufficient, indicating that the hidden layer size might be inadequate for retaining essential information for traffic accident predictions. Especially when considering the LAL outcomes, we deduce that the model might not achieve higher accuracy moving forward, as the number of "active" cells, anticipated to increase with more epochs, remains stagnant. A similar trend is visible with the results for M_{512}. In terms of AP, compared to the outcomes of M_{1024} and M_{2048}, it is clear that the training was less effective. Likewise, concerning LAL, its growth rate is slower, settling at a lower value by epoch 30. From the above, it can

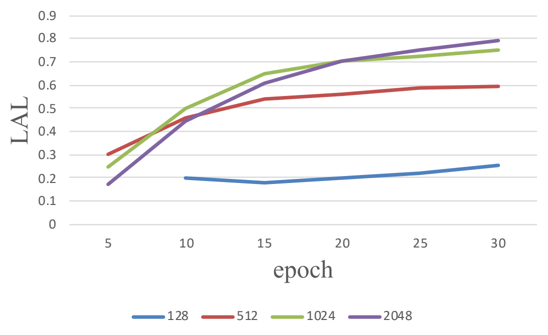

Figure 7: Epoch-wise Transition of LSTM Activity Levels (LAL) for Models M_{128}, M_{512}, M_{1024}, and M_{2048}. The plot illustrates the progression and potential stability of LAL across different model complexities and provides insights into the effective hidden layer size during the training for accident prediction.

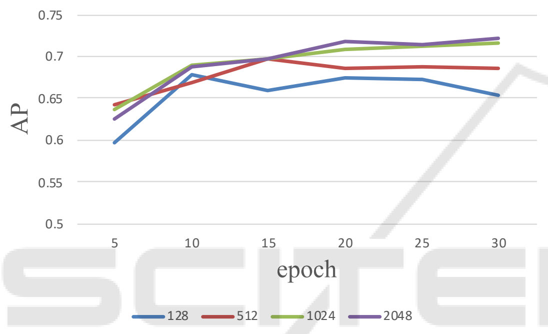

Figure 8: Epoch-wise Transition of Average Precision (AP) for Models M_{128}, M_{512}, M_{1024}, and M_{2048}. The graph demonstrates the predictive performance of each model over the epochs and aids in understanding the model's efficiency in predicting traffic accidents throughout the training process.

be inferred that for models with a hidden layer size of 128 and 512, the potential is not promising, thus in SEN, we believe that increasing the size of the hidden layer and retraining is effective.

Additionally, analyzing the results for M_{1024} and M_{2048}, both AP and LAL appear to be nearly identical. This observation leads us to conclude that augmenting the number of LSTM cells beyond this might only result in convergence to similar values, aiding in determining the optimal LSTM cells count. In other words, we consider it effective to continue training with the current parameters in SEN.

In summation, the observed relationship between the increase in LAL and AP values during training indicates that by monitoring changes in LAL values, we can discern whether to prolong training or if the current hidden layer size is promising for future accuracy enhancements.

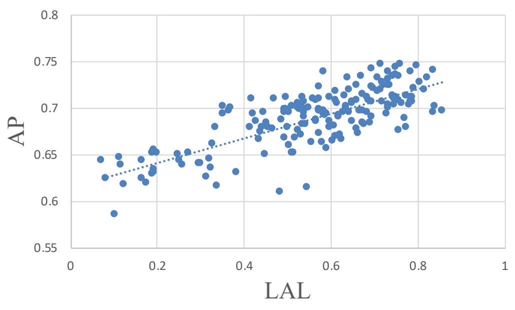

Figure 9: Correlation Analysis between LSTM Activity Levels (LAL) and Average Precision (AP). The scatter plot represents models M_{512}, M_{1024}, and M_{2048}, each at epochs 5, 10, 15, 20, 25, and 30, suggesting a significant positive correlation (0.767) that implies the potentiality of LAL as a predictive indicator of model accuracy in future epochs.

4.2.2 Correlation Between LSTM Activity Levels and Accuracy

We investigated the correlation between LAL and AP for the models M_{512}, M_{1024}, and M_{2048}. We excluded M_{128} due to its notably low LAL. Data was plotted for LAL and AP at epochs 5, 10, 15, 20, 25, and 30, for each model trained 10 times. The results are depicted in Figure 9. A correlation coefficient of 0.767 indicates a significant positive relationship. From the foregoing, we believe that by extrapolating the LAL in the early stages of training, it is possible to predict future accuracy.

However, there currently remains a challenge regarding the computational cost of LAL. The distinct aspect of the intended SEN from existing methods is that, unlike the time-consuming validation accuracy calculated per epoch with a large amount of data using AP or other evaluation methods, it employs a lightweight evaluation metric using internal states. Therefore, it's necessary to keep the computation cost of LAL low. The high computation cost stems from the fact that the validation data used for calculating AP is also employed to extract the scenes for TrueP, which is used in the calculation of LAL. It is sufficient to use only the data containing accidents to extract the scenes for TrueP. Additionally, since the LCAL histogram is created by integrating histograms of similar trends obtained for each scene being TrueP, we believe that a lesser total number of TrueP is acceptable. Hence, there is a need to experiment whether a positive correlation between LAL and accuracy can be obtained using validation data constituted only of a small number of accident-inclusive videos for the computation of LAL.

5 CONCLUSION

This study aims at efficient learning of models that balance accuracy and network scale as its goal. We are also targeting the construction of SEN, which evaluates the potential of a model utilizing the internal states of the network. In this paper, we focused on the LSTM in the traffic accident prediction network and defined the activity level of LSTM cells based on the variation in the values of the forget gate. Moreover, we assumed that a model has more potential if the proportion of high-activity LSTM cells is higher, and hence defined LAL. By checking the transition of LAL and AP, we demonstrated that the value of LAL is effective for controlling SEN. Additionally, since a positive correlation between LAL and AP was confirmed, we believed that it's possible to predict future accuracy by extrapolating LAL in the early stages of training.

In our future research, firstly, we plan to create a small validation data set for the calculation of LAL and experiment on the effectiveness of LAL calculated at a low cost. Then, we will proceed to discuss the specific methods of extrapolating LAL.

REFERENCES

Baker, B., Gupta, O., Raskar, R., and Naik, N. (2018). Accelerating neural architecture search using performance prediction. In *International Conference on Learning Representations*.

Chan, F. H., Chen, Y. T., Xiang, Y., and Sun, M. (2016). Anticipating accidents in dashcam videos. In *Asian Conference on Computer Vision*, pages 136–153.

Chen, Y., Yang, T., Zhang, X., Meng, G., Xiao, X., and Sun, J. (2019). Detnas: Backbone search for object detection. In *International Conference on Neural Information Processing Systems*.

Domhan, T., Springenberg, J. T., and Hutter, F. (2015). Speeding up automatic hyperparameter optimization of deep neural networks by extrapolation of learning curves. In *International Joint Conference on Artificial Intelligence*, pages 3460–3468.

Greff, K., Srivastava, R. K., Koutnık, J., Steunebrink, B. R., and Schmidhuber, J. (2017). Lstm: A search space odyssey. *IEEE Transactions on Neural Networks and Learning Systems*, pages 2222–2232.

Hutter, F., Kotthoff, L., and Vanschoren, J., editors (2019). *Automatic Machine Learning: Methods, Systems, Challenges*. Springer. In press, available at http://automl.org/book.

Karpathy, A., Johnson, J., and Fei-Fei, L. (2016). Visualizing and understanding recurrent networks. In *International Conference on Learning Representations*.

Klein, A., Falkner, S., Springenberg, J. T., and Hutter, F. (2017). Learning curve prediction with bayesian neural networks. In *International Conference on Learning Representations*.

Liu, C., Chen, L.-C., Schroff, F., Adam, H., Hua, W., Yuille, A., and Fei-Fei, L. (2019). Auto-deeplab: Hierarchical neural architecture search for semantic image segmentation. In *IEEE / CVF Computer Vision and Pattern Recognition Conference*.

Pascanu, R., Mikolov, T., and Bengio, Y. (2013). On the difficulty of training recurrent neural networks. In *International Conference on Machine Learning*, pages 1310–1318.

Real, E., Aggarwal, A., Huang, Y., and Le, Q. V. (2019). Regularized evolution for image classifier architecture search. In *AAAI Conference on Artificial Intelligence*.

Ren, S., He, K., Girshick, R., and Sun, J. (2015). Faster r-cnn: Towards real-time object detection with region proposal networks. In *IEEE / CVF Computer Vision and Pattern Recognition Conference*.

Swersky, K., Snoek, J., and Adams, R. P. (2014). Freeze-thaw bayesian optimization. arXiv:1406.3896.

Wang, N., Gao, Y., Chen, H., Wang, P., Tian, Z., Shen, C., and Zhang, Y. (2020). Nas-fcos: Fast neural architecture search for object detection. In *IEEE / CVF Computer Vision and Pattern Recognition Conference*.

Wistuba, M. and Pedapati, T. (2019). Inductive transfer for neural architecture optimization. arXiv:1903.03536.

Wu, B., Dai, X., Zhang, P., Wang, Y., Sun, F., Wu, Y., Tian, Y., Vajda, P., Jia, Y., and Keutzer, K. (2019). Fbnet: Hardware-aware efficient convnet design via differentiable neural architecture search. In *IEEE / CVF Computer Vision and Pattern Recognition Conference*.

Yan, S., White, C., Savani, Y., and Hutter, F. (2021). Nas-bench-x11 and the power of learning curves. arXiv:2111.03602.

Zhang, Y., Qiu, Z., Liu, J., Yao, T., Liu, D., and Mei, T. (2019). Customizable architecture search for semantic segmentation. In *IEEE / CVF Computer Vision and Pattern Recognition Conference*.

Zoph, B., Vasudevan, V., Shlens, J., and Le, Q. V. (2018). Learning transferable architectures for scalable image recognition. In *IEEE / CVF Computer Vision and Pattern Recognition Conference*.